Memorias del 2024 Congreso Nacional de Control Automático
8-11 de Octubre, 2024. Ciudad de México, México.

Estimation of Photoacustic Signals using Subspace Identification ⋆

Adrian Ginez-Alvarez * **Roberto G. Ramírez-Chavarría** *
Argelia Pérez-Pacheco **

* *Instituto de ingeniería, Universidad Nacional Autónoma de México, 04510 Ciudad de México, México (e-mail: AGinezA@iingen.unam.mx, RRamirezC@iingen.unam.mx)*
** *Unidad de Investigación y Desarrollo Tecnológico, Hospital General de México "Dr. Eduardo Liceaga", 06726 Ciudad de México, México (e-mail: argeliapp@ciencias.unam.mx)*

Abstract: This work presents a new estimation scheme for photoacoustic signals and the absorption profiles associated with these signals, based on a discrete linear time-invariant state-space model of the Stokes' equation, which describes the propagation of ultrasound waves in acoustic attenuating media. Parameter estimation is performed using the N4SID method for subspace identification, taking advantage of discrete model properties. In addition, the gradient descent and regularization method is used to improve parameter estimation. The simulation results validate the scope of the proposed scheme.

Keywords: Photoacustic Signals, Absorption Profile Estimation, Subspace Identification, Linear State Space Model, Parameter and State Estimation

1. INTRODUCTION

The photoacoustic effect occurs when a sample capable of absorbing optical energy is exposed to a laser, causing its temperature to increase. As a result, the sample expands due to the absorbed energy. In its natural search for thermal equilibrium with the environment, the sample subsequently contracts. This process generates disturbances in the shape of waves in the propagation medium, which are captured by an array of ultrasound detectors positioned near the sample (Veloz (2023)). These detectors transmit information to a computer responsible for reconstructing the optical absorption, ultimately generating a photoacoustic image (Lang et al. (2019)), see Fig. 1. The optical absorption profile obtained from the photoacoustic image provides valuable information about the distribution of chromophores within the sample. By analyzing this profile, it is possible to detect the sample's internal structures. Therefore, this profile is the key in the reconstruction of photoacoustic imaging, along with the measured pressure signal.

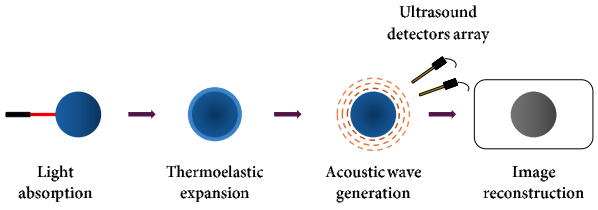

Fig. 1. Representation of Photoacoustic effect

⋆ This work was supported by UNAM-PAPIIT TA101423.

This work builds on Lang et al. (2019) proposal to approach the photoacoustic effect from a State-Space Model (SSM), but modifies the way of recovering the absorption profile of a sample from measurements through subspace identification. In addition, the gradient descent and regularization method is used to improve parameter estimation. By making this modification for parameter estimation, it is possible to work with noisy measurement data. On the other hand, the SSM allows generating an output signal that is compared with the measurements to validate the estimation of the absorption profile. This article is organized as follows: Section 2 describes the model used and the techniques employed to improve parameter estimation. Section 3 describes the proposed estimation scheme. Finally, the simulation results are presented in Section 4.

2. THEORETICAL BACKGROUND

2.1 Ultrasound detector discretization

The depth in the ultrasound detector is defined by z, N_z represents the number of divisions in the detector, Δ_z represents the spacing between each division, and Δ_t represents the temporal discretization value, see Fig. 2.

2.2 State-Space Model

Starting from the Stokes' equation, which describes the propagation and attenuation of the acoustic wave as a function of depth and time,

$$\frac{\partial^2 p(z,t)}{\partial z^2} - \frac{1}{c_0^2}\frac{\partial^2 p(z,t)}{\partial t^2} + \tau \frac{\partial^3 p(z,t)}{\partial t \partial z^2} = -\frac{\beta}{C_p}\frac{\partial H(z,t)}{\partial t}, \quad (1)$$

https://doi.org/10.58571/CNCA.AMCA.2024.071

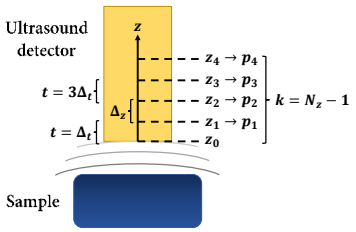

Fig. 2. Representation of the discretization

where $p(z,t)$ represents the local pressure at z, c_0 is the speed of sound in the propagation medium, τ is the relaxation time, C_P is the specific heat, and β is the thermal expansion coefficient of the sample. The vector $p_k \in \mathbb{R}^{N_z \times 1}$ is defined as:

$$p_k = \begin{bmatrix} p_0(z_0,t) \\ p_1(z_1,t) \\ \vdots \\ p_{N_z-1}(z_{N_z-1},t) \end{bmatrix} \quad ; \quad k = N_z - 1,$$

where p_k is the set of local pressures at depth z at time $t = k\Delta_t$. Meanwhile, $H(z,t)$ is a heating function that describes the density of optical energy absorbed per unit of time at a certain depth (Lang et al. (2019)). It can be written as the product of a position-dependent function $R(z)$ and a time-dependent function $i(t)$,

$$H(z,t) = R(z)i(t), \tag{2}$$

where $R(z)$ is the optical energy absorption and $i(t)$ is the temporal illumination profile. The central finite difference method is used to discretize each term of Eq.(1) as:

$$\frac{\partial^2 p(z,t)}{\partial z^2} \approx G p_k, \tag{3}$$

$$-\frac{1}{c_0^2}\frac{\partial^2 p(z,t)}{\partial t^2} \approx -\frac{1}{c_0^2\Delta_t^2}\left(p_{k+1} - 2p_k + p_{k-1}\right), \tag{4}$$

$$\tau\frac{\partial^3 p(z,t)}{\partial t \partial z^2} \approx \tau\frac{1}{2\Delta_t} G(p_{k+1} - p_{k-1}), \tag{5}$$

$$-\frac{\beta}{C_p}\frac{\partial h_k}{\partial t} \approx r u_k, \tag{6}$$

with

$$G = \frac{1}{\Delta_z^2}\begin{bmatrix} -2 & 1 & 0 & 0 & 0 & \dots & 0 \\ 1 & -2 & 1 & 0 & 0 & \dots & 0 \\ 0 & 1 & -2 & 1 & 0 & \dots & 0 \\ \vdots & & \ddots & \ddots & \ddots & & \vdots \\ 0 & \dots & 0 & 1 & -2 & 1 & 0 \\ 0 & \dots & 0 & 0 & 1 & -2 & 1 \\ 0 & \dots & 0 & 0 & 0 & 1 & -2 \end{bmatrix},$$

$$r = -\frac{\beta\chi}{C_p\Delta_t} m, \tag{7}$$

and

$$u_k = i_s - i_{s-1}, \tag{8}$$

where $G \in \mathbb{R}^{N_z \times N_z}$ and i_s is the continuous laser intensity. While h_k is the discretization of Eq.(2) that follows:

$$h_k \approx \chi \underbrace{\begin{bmatrix} \mu_0 \\ \mu_1 a_0 \\ \vdots \\ \mu_{N_z-1} a_{N_z-2} a_{N_z-3} \dots a_1 a_0 \end{bmatrix}}_{m} i_s, \tag{9}$$

where $m \in \mathbb{R}^{N_z \times 1}$ and $\mu_n \in \mathbb{R}^{N_z \times 1}$ for $n = 0, \dots, N_z - 1$ is
the discretized absorption profile of the ultrasound detector. The term $a_n = e^{-\mu_n \Delta_z}$ approximately describes the attenuation of the laser intensity through z.

By substituting equations (3), (4), (5) and (6) into equation (1), and grouping the coefficients into matrices $M \in \mathbb{R}^{N_z \times N_z}$ to simplify notation,

$$\overbrace{\left(-\frac{1}{c_0^2\Delta_t^2}I + \frac{\tau}{2\Delta_t}G\right)}^{M_1} p_{k+1} + \overbrace{\left(G + \frac{2}{c_0^2\Delta_t^2}I\right)}^{M_2} p_k + \overbrace{\left(-\frac{1}{c_0^2\Delta_t^2}I - \frac{\tau}{2\Delta_t}G\right)}^{M_3} p_{k-1} = r u_k,$$

$$M_1 p_{k+1} + M_2 p_k + M_3 p_{k-1} = r u_k, \tag{10}$$

a linear equation is obtained that relates the pressure profiles p_k, p_{k-1} and p_{k+1} with the input u_k, which represents the pressure generation in response to the laser signal. Solving p_{k+1} from Eq.(10),

$$p_{k+1} = \overbrace{(-M_1^{-1}M_2)}^{A_{11}} p_k + \overbrace{(-M_1^{-1}M_3)}^{A_{12}} p_{k-1} + \overbrace{M_1^{-1}r}^{f} u_k,$$

$$p_{k+1} = A_{11}p_k + A_{12}p_{k-1} + f u_k. \tag{11}$$

Define the state vector $x_k \in \mathbb{R}^{2N_z \times 1}$ as:

$$x_k = \begin{bmatrix} p_k \\ p_{k-1} \end{bmatrix}, \tag{12}$$

to formulate a SSM. Therefore

$$\begin{bmatrix} p_{k+1} \\ p_k \end{bmatrix} = \begin{bmatrix} A_{11} & A_{12} \\ I & 0 \end{bmatrix}\begin{bmatrix} p_k \\ p_{k-1} \end{bmatrix} + \begin{bmatrix} f \\ 0 \end{bmatrix} u_k, \tag{13}$$

$$x_{k+1} = Ax_k + Bu_k, \tag{14}$$

where A_{11} y $A_{12} \in \mathbb{R}^{N_z \times N_z}$, $A \in \mathbb{R}^{2N_z \times 2N_z}$, $f \in \mathbb{R}^{N_z \times 1}$ and $B \in \mathbb{R}^{2N_z \times 1}$. If c_0, τ, Δ_t, $\Delta_z \in \mathbb{R}^+$, the matrix A is stable (Lang et al. (2019)). Given that the measurements are obtained by the detector at the surface ($z = 0$), to complete the model, the following output equation is defined:

$$y_k = Cx_k, \tag{15}$$

where $C \in \mathbb{R}^{1 \times 2N_z}$ with $C(1,1) = 1$ and the rest of the vector is zero. Additionally, considering process noise w_k and measurement disturbances v_k, the discrete linear SSM is represented by the following equations:

$$x_{k+1} = Ax_k + Bu_k + w_k, \tag{16}$$

$$y_k = Cx_k + v_k, \tag{17}$$

where y_k is the photoacustic signal. However, it is not possible to directly construct the input matrix B because its relationship with the absorption profile in Eq.(9) requires the vector μ_n to be previously known.

2.3 N4SID

Hankel matrix is the foundation of subspace identification algorithms, as this matrix can be easily constructed from the available input-output data. The block Hankel matrix is defined as:

$$\mathcal{H} = \left[\begin{array}{cccc} h_0 & h_1 & \dots & h_{j-1} \\ \vdots & \vdots & \ddots & \vdots \\ h_{i-1} & h_i & \dots & h_{i+j-2} \\ \hline h_i & h_{i+1} & \dots & h_{i+j-1} \\ \vdots & \vdots & \ddots & \vdots \\ h_{2i-1} & h_{2i} & \dots & h_{2i+j-2} \end{array}\right] = \begin{bmatrix} H_p \\ H_f \end{bmatrix}, \tag{18}$$

where $H_p \in \mathbb{R}^{li\times j}$, $H_f \in \mathbb{R}^{li\times j}$, the subscripts p and f denote past and future data, respectively. The sequences of input and output measurements are arranged in block Hankel matrices U and Y. The number of matrix rows i is a sufficiently large index defined by the user, meaning it must be at least greater than the maximum order of the system to be identified (Overschee and Moor (1996)). The number of columns j indicates the number of measurements.

The N4SID algorithm (*Numerical algorithms for Subspace State Space System IDentification*) estimates a SSM with the structure:

$$x_{k+1} = Ax_k + Bu_k,$$
$$y_k = Cx_k + Du_k,$$

only using u_k and y_k. The estimation starts by constructing a block Hankel matrix for the input, output, and system state following the structure of Eq.(18). Additionally, for the output, it is important to generate the projection of the future output space Y_f onto the past output space Y_p,

$$\mathcal{O}_i = \frac{Y_f}{Y_p}, \tag{19}$$

where $\mathcal{O}_i$ is the oblique projection of the output space. Afterwards, a Singular Value Decomposition (SVD) of $\mathcal{O}_i$ is required to stimate the order of the SSM, as follows:

$$W_1\mathcal{O}_iW_2 = U\mathcal{S}V^T, \tag{20}$$

where W_1 and W_2 are weighting matrices for the singular values, $U \in \mathbb{R}^{m\times n}$ and $V \in \mathbb{R}^{n\times n}$ are orthogonal matrices, and $\mathcal{S} \in \mathbb{R}^{n\times n}$ is the diagonal matrix of singular values.

On the other hand, let be $\Gamma_i \in \mathbb{R}^{li\times n}$ the extended observability matrix defined as

$$\Gamma_i = \begin{bmatrix} C & CA & CA^2 & \dots & CA^{i-1} \end{bmatrix}^T, \tag{21}$$

and the estimated state sequence

$$\hat{X}_i = (\hat{x}_i \quad \hat{x}_{i+1} \quad \cdots \quad \hat{x}_{i+j-1}),$$

the projection $\mathcal{O}_i$ is given by

$$\mathcal{O}_i = \Gamma_i\hat{X}_i. \tag{22}$$

Following the SVD in Eq.(20), Using the singular values of $\mathcal{O}_i$ it is possible to reconstruct Γ_i, since the output space is related to the input space, then

$$\Gamma_i = W_1^{-1}U\mathcal{S}^{1/2}, \tag{23}$$
$$\Gamma_{i-1} = \Gamma_i. \tag{24}$$

The estimation of $\hat{X}_i$ is calculated as follows:

$$\hat{X}_i = \Gamma_i^\dagger\mathcal{O}_i, \tag{25}$$

where the symbol † denotes the pseudo-inverse of the observability matrix. Therefore, for each time instant, the last row of Γ_i is removed until reaching Γ_{i-1}. Starting from this, the next sequence of states, $\hat{X}_{i+1} = (\hat{x}_{i+1} \quad \hat{x}_{i+2} \quad \cdots \quad \hat{x}_{i+j})$, is determined as follows:

$$\hat{X}_{i+1} = \Gamma_{i-1}^\dagger\mathcal{O}_{i+1}, \tag{26}$$

where O_{i-1}, is formed by shifting the first block row of Y_f to the last row of Y_p, following the structure of Eq.(18) for the output y.

After recovering the observability matrix and the sequence of states, the estimation of the state-space system matrices is performed by formulating the following linear problem:

$$\begin{bmatrix} \hat{X}_{i+1} \\ Y_{i|i} \end{bmatrix} = \begin{bmatrix} A & B \\ C & D \end{bmatrix}\begin{bmatrix} \hat{X}_i \\ U_{i|i} \end{bmatrix} + \begin{bmatrix} W \\ V \end{bmatrix}, \tag{27}$$

where $Y_{i|i}$ is a block Hankel matrix with only one row of outputs, W is the process noise, and V is the measurement disturbance (Pérez-Pacheco et al. (2024)). Considering that W and V are white noise sequences with zero mean, uncorrelated with the system states, the solution to Eq.(27) for the state-space matrices is formulated as a least squares approximation:

$$\underset{\hat{\mathscr{L}}}{min} \left\| \begin{bmatrix} \hat{X}_{i+1} \\ Yi|i \end{bmatrix} - \hat{\mathscr{L}}\begin{bmatrix} \hat{X}_i \\ U_{i|i} \end{bmatrix} \right\|_F^2, \tag{28}$$

$$\hat{\mathscr{L}} = \begin{bmatrix} A & B \\ C & D \end{bmatrix}. \tag{29}$$

State-space matrices are not computed in their canonical forms, but rather as complete state-space matrices (Overschee and Moor (1994)).

2.4 Gradient descent

Gradient descent is an optimization algorithm that seeks to estimate the parameter values that minimize a cost function $J(\theta)$. Iteratively, the values of θ are adjusted in the direction that most reduces the cost function (Ruder (2016)). In other words, the gradient of the function with respect to θ is calculated, and the values are updated according to:

$$\theta = \theta - \alpha\nabla J(\theta) \tag{30}$$

where α is the learning rate, which determines the size of the adjustment in each iteration.

2.5 Regularization

Regularization is a technique to reduce uncertainty in parameter estimation, avoiding overfitting in models derived from measurements. It also allows setting previously known values of the model parameters to maintain physical validity. Regularization modifies a cost function by adding a penalty term. Unlike the gradient descent method, θ is obtained by minimizing the following cost function:

$$J_R(\theta) = \frac{1}{N}\sum_{k=1}^{N}\varepsilon^2(k,\theta) + \frac{1}{N}\lambda\theta^T P\theta, \tag{31}$$

where N is the number of measurement data points, $\varepsilon(k,\theta)$ is the prediction error between the measurement and the model estimation, λ is a positive constant that balances bias (systematic error) and variance (uncertainty

in the estimates): the higher the value of λ, the greater the bias and the lower the variance of θ, and P is a positive definite matrix that helps maintain model stability and incorporate known information about the parameters (Ljung (2013)).

3. ESTIMATION SCHEME

3.1 Parametric estimation

Assuming the discretization parameters of the model and the sample parameters, both condensed in Table 1, are known, and given a set of measurements of a photoacoustic signal $y(k) = [y(k_0),\ y(k_1),\ ...,\ y(k_w)]'$ and the associated laser signal $u(k) = [u(k_0),\ u(k_1),\ ...,\ u(k_w)]'$, where w is the total number of measurements, the estimation of the parameters in the matrix B is formulated using subspace identification, specifically through the N4SID algorithm. The parameters are then adjusted using the gradient descent method by least squares and regularization.

Table 1. Parameters required for estimation

Parameter	Unit
Δ_z	m
N_z	u
Δ_t	s
τ	s
χ	u
c_0	m/s
β/C_P	u

As a prior step to identification, it is necessary to define an estimated input matrix $\hat{B} \in \mathbb{R}^{2N_z \times 1}$ as:

$$\hat{B} = \begin{bmatrix} \hat{f} \\ 0 \end{bmatrix}. \tag{32}$$

Extracting the vector $\hat{f}$ from Eq.(32) and using Eq.(7),

$$\hat{f} = M_1^{-1}\hat{r}, \tag{33}$$

$$\hat{f} = M_1^{-1}\left(-\frac{\beta\chi}{C_p\Delta_t}\hat{m}\right). \tag{34}$$

Solving $\hat{m}$ from the previous equation,

$$\hat{m} = -\frac{C_p\Delta_t}{\beta\chi}M_1\hat{f}, \tag{35}$$

it is possible extract the estimated absorption profile $\hat{\mu}_n \in \mathbb{R}^{N_z \times 1}$ from (9) as follow:

$$\hat{\mu}_n = \frac{\hat{m}_n}{\Pi_{i=0}^{n-1}\hat{a}_i}. \tag{36}$$

The equation (36) highlights that the reconstruction of $\hat{\mu}_n$ completely depends on subspace identification, which in turn relies on the quality of the available measurements.

It is considered that the generation of photoacoustic signals (see Fig.1) is a controlled process that begins with a sample not excited by laser illumination, ensuring that the initial conditions in the experiment are null, i.e., $x_0 = 0$. The estimation of the matrix $\hat{B}$ requires the construction of the matrices A and C to use subspace identification and ensure that the values determined by the algorithm retain physical meaning with the photoacoustic effect. Thanks to this, the identification algorithm does not require determining the model order through SVD, and the accuracy of the estimation depends solely on the amount of available data and the reduction of noise in the measurements to achieve convergence. However, the computational load of the proposed scheme directly depends on the choice of N_Z, as the order of the models is $2N_Z$. The implementation of the N4SID algorithm and its adjustment via gradient descent and regularization was carried out in MATLAB™ R2023b, using a set of input-output data $[u_k \quad y_k]$ to form the block Hankel matrices. This set is considered as experimental data. The estimated matrix model follows the structure of equations (16) and (17), which is rewritten as follows:

$$\hat{x}_{k+1} = A\hat{x}_k + \hat{B}u + w_k, \tag{37}$$

$$\hat{y}_k = C\hat{x}_k + v_k, \tag{38}$$

where $\hat{B} \in \mathbb{R}^{2N_z \times 1}$ is initialized in $\hat{B} = 0$ and $\hat{x}_0 = 0$.

After solving equation (28) for $\hat{B}$, with $\hat{B}$ being the only unknown ($D = 0$), the input matrix values are adjusted according to equations (30) and (31) due to the presence of noise in the measurements. This noise was considered as white noise $\mathcal{N}(0, 0.25)$ and $w_k = 0$.

3.2 Photoacustic signals estimation

Starting from the matrix $\hat{B}$, the estimated matrix model is simulated using u_k to generate the estimated photoacoustic signal $\hat{y}_k$.

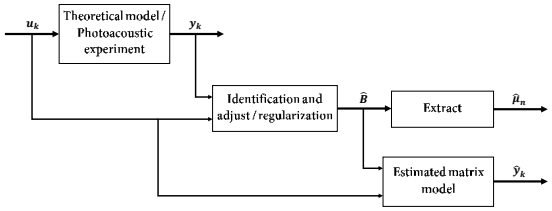

Fig. 3. Diagram of the Estimation Scheme

The estimated photoacustic signal $\hat{y}_k$ and reconstruction of the sample's absorption profile $\hat{\mu}_n$ follow the workflow shown in Fig. 3.

4. SIMULATION EXAMPLES

This section aims to demonstrate the generation and estimation of photoacoustic signals from the discrete model through the simulation of two photoacoustic experiments. A comparison is made between the experimental photoacoustic signal and the estimated signal for each estimated absorption profile. The discretization parameters and input signal were taken from Lang et al. (2019) and summarized in Tables 2 and 3. A sampling time, t_s, of 0.1 s and a simulation time, t_f, of 50 s were considered. The input signal in Fig.4c represents a short laser pulse, usually used in Photoacustic.

4.1 Example 1

This experiment aims to demonstrate the performance of the proposed scheme for parameter estimation and

Table 2. Model simulation parameters

Parameter	Value
Δ_t	1×10^{-9} s
Δ_z	3×10^{-6} m
N_z	20

Table 3. Example simulation parameters

Parameter	Value
t_f	50 s
i_k	$f(k\|6, 2)$
x_k	0
τ	77×10^{-12} s
χ	0.03
c_0	1500 m/s
β/C_P	1/1

photoacoustic signal estimation in the absence of noise in the measurement data. Figure 4 shows the estimation of the absorption profile and the estimation error in each layer, as well as the input signal of the dataset $[u_k \quad y_k]$ used to generate the photoacoustic signal from the estimated matrix model. The absorption profile used for this experiment implies that the internal structures of the sample have a high degree of optical absorption, which facilitates the identification of their distribution. Figure 4a shows that the estimation of μ_n is quite good, and Figure 4b supports this statement.

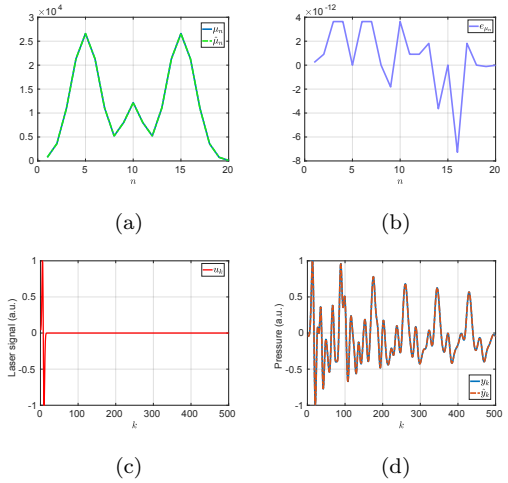

Fig. 4. (a): Absorption Profile estimation. (b): Estimation error of μ_n. (c): Input signal u_k. (d): Photoacoustic Signal estimation without noise

However, in a real experiment, it is not possible to compare $\hat{\mu}_n$, so it is necessary to simulate the system response $\hat{y}_k$ and compare it with the signal y_k to validate the profile estimation, as seen in Fig. 4d. Note that both y_k and $\hat{y}_k$ are available signals. Using the `compare()` function in MATLAB™, a 100% similarity between the two signals is obtained, demonstrating that in the absence of noise in the measurement data, the proposed scheme has a high level of estimation accuracy.

4.2 Example 2

This experiment aims to demonstrate the advantages of using a state-space model to represent a physical phenomenon and the effect of regularization in the presence of noise in the measurements. A lower magnitude absorption profile is used compared to that in Example 1 (see Figure 4a) and white noise is added to the measurements $\mathcal{N}(0, 0.25)$ and $w_k = 0$. Additionally, N_z is modified to 50 to obtain a smoother absorption profile. Figure 5 shows the estimation results for a short pulse as the input signal without regularizing the parameters adjusted by gradient descent. Figures 5a and 5b show a very poor estimation of μ_k and y_k, respectively, due to the Signal-to-Noise Ratio (SNR) being -40.96 dB. In this case, the gradient descent method causes overfitting in the parameter estimation due to the high level of noise in the measurements. The estimation improves considerably with the use of regularization, with $\lambda = 250$, as shown in Figures 6a and 6b. However, the input signal and absorption level limit the quality of the results as the y_k signal remains corrupted by noise.

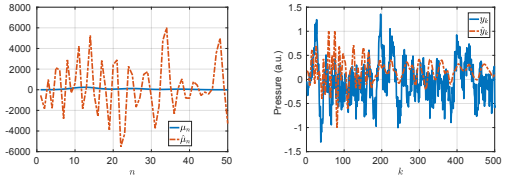

Fig. 5. (a): Absorption Profile estimation without regularization. (b): Photoacoustic Signal estimation with noise

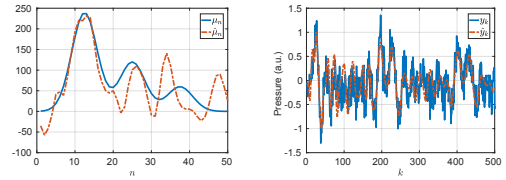

Fig. 6. (a): Absorption Profile estimation with regularization. (b): Photoacoustic Signal estimation with noise

Signal intput modification The state-space representation of the photoacoustic effect allows modifying the input signal to achieve a better estimation of the absorption profile without the need to physically modulate the laser signal and compromise the sample's characteristics. By approximating the behavior of $\hat{\mu}_n$ (see Figure 6a), the input signal is modified by a sinusoidal signal $u_k = sin(0.5t_s)$, representing the prolonged exposure of the sample to a series of long pulses, as observed in Figure 7c. This modification improves the estimation of the absorption profile since the SNR reaches a value of 3.98 dB under the same noise conditions established previously. Figures 7a and 7b show that the estimation is sufficiently reliable despite the low absorption level, especially from layer 30 onward. On the other hand, the estimation error slightly affects the photoacoustic signal generated by the model, as seen in Figure 7d. The regularization of the parameters does not have a noticeable impact on the es-

https://doi.org/10.58571/CNCA.AMCA.2024.071

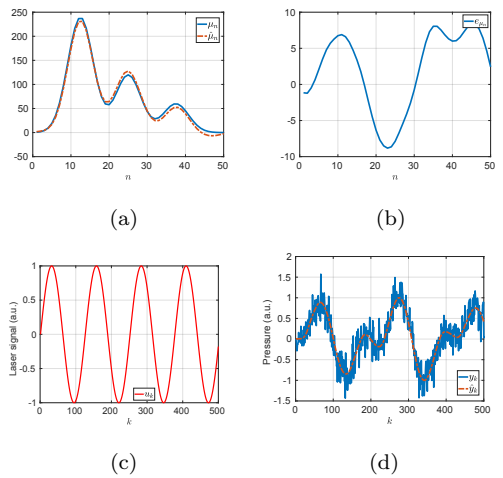

Fig. 7. (a): Absorption Profile estimation. (b): Estimation error of μ_n. (c): Input signal u_k. (d): Photoacustic Signal estimation with noise

timation of μ_n or y_k, and therefore it is not implemented. The condition for applying regularization and selecting the value of λ primarily depends on whether the SNR value is negative. Additionally, the selection of u_k must make physical sense; otherwise, the signal $\hat{y}_k$ will not be bounded, and the values of $\hat{\mu}_n$ will not be reliable. Finally,

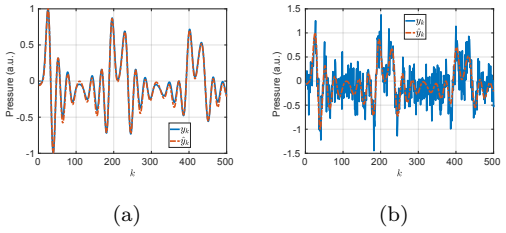

Fig. 8. (a): Photoacustic Signal estimation without noise. (b): Photoacustic Signal estimation with noise

the estimated matrix model, which allowed the extraction of the estimated profile in Figure 7a, is used to generate the corresponding photoacoustic signal for a short pulse as the input signal. Figure 8a shows the measured photoacoustic signal y_k without noise and the estimated signal $\hat{y}_k$ to highlight that the estimation error of μ_n directly affects $\hat{y}_k$. Therefore, it is important to reduce this error to perform tests with different input signals. In Figure 8b, it can be seen that the photoacoustic signal generated by the model best fits the signal contaminated with an SNR of -40.96 dB, compared to Figures 5b and 6b. Note that using the model to generate a photoacoustic signal associated with a specific input is not merely an illustrative exercise, as the contaminated signal is actually the only available information that also allows validation of the estimation performed with the sinusoidal signal.

5. CONCLUSIONS

A solution to the inverse photoacoustic problem has been presented from a dynamic systems perspective, capable of recovering the absorption profile of an optically absorbent sample and generating a photoacoustic signal very similar to that captured by the detector. This solution is based on the SSM derived from the Stokes' equation proposed by Lang et al. (2019), which describes the propagation and attenuation of the acoustic wave. Additionally, due to finite difference discretization, the model's matrices have constant parameters, reducing computational cost without compromising estimation accuracy. This accuracy could be further improved with a more precise numerical method, although at the expense of complicating the SSM. After analyzing the unknown parameters in the model and the availability of experimental data, subspace identification was used to approximate these parameters. Subsequently, using the gradient descent algorithm, the parameters were readjusted until a response similar to the measurements was achieved. The proposed scheme allows for testing different modulations of the laser signal to enhance the signal generated by the SSM, and it facilitates structured subspace identification that focuses the estimation on a single matrix, thereby achieving a good estimation of B in high-order systems. However, depending on the SNR value, it was necessary to regularize the parameters to compensate for the effects of noise. An alternative method to subspace identification is the use of a linear regressor approach, but this option is more sensitive to noise in the measurements and requires the implementation of optimization methods. Additionally, this solution does not leverage the benefits of the SSM. The experimental results suggest that the proposed scheme is promising for generating photoacoustic images. All the experiments presented in this work can be considered theoretical results until the estimation scheme is evaluated with real data from a photoacoustic experiment.

It should be noted that comparing the obtained results with other methods is beyond the scope of this work.

REFERENCES

Lang, O., Kovács, P., Motz, C., Huemer, M., Berer, T., and Burgholzer, P. (2019). A linear state space model for photoacoustic imaging in an acoustic attenuating media. *Inverse Problems*, 35(1), 015003.

Ljung, L. (2013). Some classical and some new ideas for identification of linear systems. *Journal of Control, Automation and Electrical Systems*, 24(1), 3–10.

Overschee, P.V. and Moor, B.D. (1994). N4sid: Subspace algorithms for the identification of combined deterministic-stochastic systems. *Automatica*, 30(1), 75–93.

Overschee, P.V. and Moor, B.D. (1996). *Subspace Identification for Linear Systems: Theory, Implementation, Applications*. Kluwer Academic Publishers.

Pérez-Pacheco, A., Ramírez-Chavarría, R.G., Quispe-Siccha, R.M., and Colín-García, M.P. (2024). Dynamic modeling of photoacoustic sensor data to classify human blood samples. *Medical & Biological Engineering & Computing*, 62(2), 389–403.

Ruder, S. (2016). An overview of gradient descent optimization algorithms. *arXiv preprint arXiv:1609.04747*.

Veloz, G.M.R. (2023). *Novel reconstruction algorithm for photoacoustic imaging: toward the quantitative imaging*. Ph.D. thesis, Universidad de Guanajuato.

